Chapter I.2
Meteorological Radar Systems

Mario Montopoli and Frank S. Marzano

1 Introduction

During the beginning of 1941, while someone were trying to eliminate natural meteorological echoes from radar returned signals to better distinguish moving manmade sensible targets, others were attempting to study them. It was the beginning of the radar era within the meteorological context.

The first studies were addressed in identifying the rain formation, whereas quantitative rain estimation were available only around 1960 (see Atlas, 1954).

Nowadays, radar systems are quite diffuse instrument with multiple applications and products which are continuously improved both by hardware innovations and by algorithms developments. Most diffuse radar systems are labeled with the term "weather radars" which are mainly ground-based systems. They are able to detect radar signal from precipitating droplets in different phases which are basically rain, ice, and snow of variable sizes (of the order of 1–10 mm) and shapes. Weather radars operates at wavelengths from about 15 cm to 3 cm (i.e., between 2 and 10 GHz respectively) and, as will be discussed later, they have, in their advanced configuration, Doppler and polarization capability which means that they can measure radial wind speed and classify the shape and type of the sensed hydrometeors (Vivekanandan et al. 1999; Baldini et al. 2004; Gorgucci et al. 2002; Marzano et al. 2006; Vivekanandan et al. 2004; Zrnic et al. 2001).

The perspective from the ground has several advantages but suffers from too limited spatial coverage (i.e., nearly 200 km with 1 km resolution) to observe large rain formations. Radar from satellite tends to compensate the above-mentioned problem but many additional challenging problems rise, including cost, size constraints, reliability issues, and temporal sampling. It is obviously impossible to continuously sample every precipitating cloud from radar orbiting the Earth. An example of space-borne precipitation radar (PR) is aboard of the Tropical Rainfall Measuring Mission (TRMM) satellite launched in 1997 (Toshiaki et al., 2009).

M. Montopoli (✉)
Centre of Excellence CETEMPS and Department of Electrical and Information Engineering, University of L'Aquila, L'Aquila, Italy
e-mail: mario.montopoli@univaq.it

D. Cimini et al. (eds.), *Integrated Ground-Based Observing Systems*,
DOI 10.1007/978-3-642-12968-1_2, © Springer-Verlag Berlin Heidelberg 2010

The precipitation radar was the first space-borne instrument designed to provide three-dimensional maps of storm structure. It operates at 2-cm wavelength (i.e., 15 GHz) and it has a swat width of 247 km with a resolution of 5 km. These measurements yield needful information on the intensity and distribution of the rain, on the rain type, on the storm depth, and on the height at which the snow melts into rain. The estimates of the heat released into the atmosphere at different heights based on these measurements can be used to improve models of the global atmospheric circulation.

Radars to study precipitations are not the unique existing radar systems. Another class of radars, called cloud radars, are designed to monitor cloud structure with wavelengths about 10 times shorter than those used in conventional storm surveillance radars, i.e., at 8.6 mm or 3.3 mm or in frequency domain, respectively, at 35 and 90 GHz. When installed on the ground, they monitor clouds which pass over the radar site or in other words they are vertically pointed. When installed on space platform they are nadir looking as in the case of cloud profiling radar (CPR) aboard of CloudSat space platform (Graeme et al., 2002).

These types of radars are aimed to estimate the cloud boundaries (e.g., cloud bottoms and tops) and due to the shorter wavelength used, they are able to detect tiny water and ice droplets that conventional radars are unable to sense. The cloud radar also helps to estimate microphysical properties of clouds, such as particle size and mass content, which help to understand how clouds interact with radiant energy passing though the atmosphere.

Radar are also those operating at wavelengths from 30 cm to 6 m, mainly used to probe the clear air or regions without clouds where the airflow characteristics can be determined up to 10 km above the Earth's surface. For these applications radars are known as profilers. The basic principle is that the gradient variations of index of refraction of air, that is quantity observed by the profiler, are connected to small fluctuations in air temperature and moisture content.

Eventually, belong to the class of radars are also those operating at optical frequencies as LIDARs, used to accomplish studies on aerosol particles and air molecules and allowing air motions to be determined, especially in thin, high tropospheric clouds, and in the Earth's boundary layer (approximately the lowest 1 km of the Earth's atmosphere)

This chapter attempts to give the reader the basic principles of radar systems, first introducing concepts which are common to all radar categories and second focusing the discussion on weather radar polarimetry of precipitation. Throughout the chapter, the ground-based perspective will be followed in order to facilitate the comprehension of the basic concepts without introducing the complication of the geometry of observation.

2 Radar Systems

Precipitation radars are widely used to determinate the location, size, and intensity of rain formation. Ground-based scanning precipitation radars are used in short-term weather and flood forecasting, to estimate the distribution and the amount

of cumulative rainfall over a region (typically of 200×200 km^2) and thanks to polarimetric radars to classify the types of hydrometeors. Weather radars of many countries have networks of operational radars that monitor precipitation near population centers [see a Europe and American example in Holleman et al. (2008), Saffle et al. (2002), and Alberoni et al. (2002)]. The output of these operational radar networks can be combined to provide a picture of the distribution of precipitation over synoptic-scale regions. Precipitation radars, developed by the British and Americans during the World War II, are also used to map the three-dimensional structure of storms.

Radars transmit a pulse of electromagnetic energy, by means of an antenna, and when the transmitted energy encounters a particle, such as, for example, a raindrop for water radars, part of the transmitted energy is scattered back toward the antenna where it is received and amplified. The time delay between the original pulse transmission and the receipt of the backscattered energy is used to deduce the distance to the reflector antenna. The frequency used by weather radars is divided into several bands which are usually S band (2–4 GHz), C band (4–8 GHz), and X band (8–12 GHz) for ground-based station, and Ku (12–18 GHz) and Ka (27–40 GHz) bands for mobile and spaceborne radars (Chandrasekar et al., 2008). On the other hand, for cloud radars, the frequencies of interest are 35 and 90 GHz.

The choice of the frequency for precipitating radar is a trade off between the practical constraints of size, weight, cost, and the relation between the wavelength and the size of the target hydrometeors. Theoretical considerations favor the choice of the longer wavelength at S and C bands for many precipitation applications. However, the use of these longer wavelengths is not always practical. The beam width for aperture antennas is proportional to λ/D_a, where D_a is the antenna diameter. In comparison to shorter wavelengths, longer ones necessitate of a larger antenna to obtain a focused beam of the same angular aperture (typically of the order of 1°). Larger antennas are heavier, require more powerful motors to move them, and are more expensive than smaller ones.

In the next sections a typical block diagram of a weather radar system will be discussed together with the derivation of the fundamental equations and the basic observable definitions and their physical significance.

2.1 Radar Scheme

The precipitation radar principally consists of a transmitter, a receiver, a transmitter/receiver switch (or circulator), and an antenna. Fig. I.2.1 shows a typical block diagram of a weather radar. The transmission section (blocks on the left side of the circulator) consists of a pulse modulator that switches the continuous sinusoidal waveform, generated by the STAble Local Oscillator (STALO) and the COHerent Oscillator (COHO), on and off to form discrete pulses. The radar sends out a pulse of a prescribed time width (T_0) and then switches to the receiver section (blocks below the circulator) to listen for possible radar echoes. The range to the targets is obtained by comparing the instants of transmission of pulses with the instants where the backscattered signal is received. In precipitation radars, the pulses are

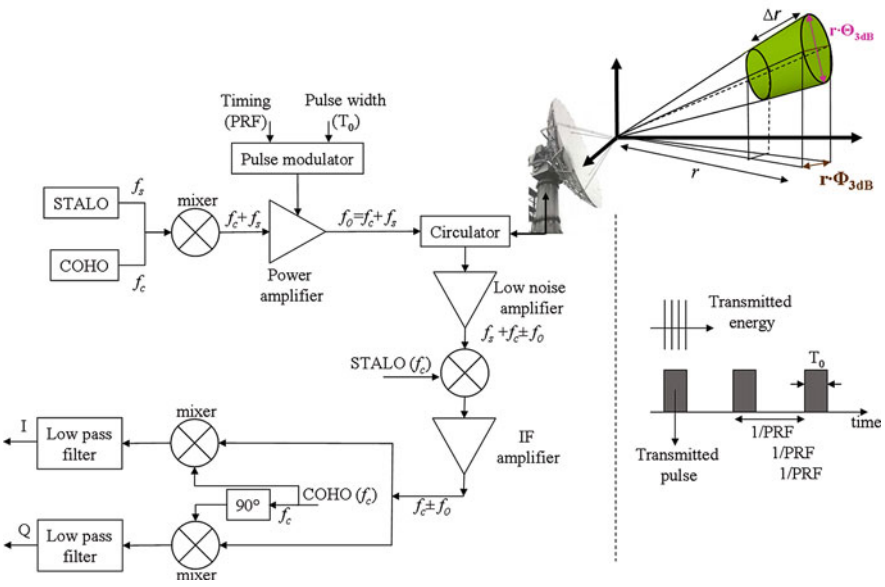

Fig. I.2.1 Block diagram of a weather radar partially taken from Bringi and Chandrasekar (2001)

transmitted at a pulse repetition frequency (PRF) of about 300–2,500 Hz and each pulse time duration is of the order of 10^{-6} s. The time interval between successive transmitted pulses limits the maximum range ($r_{\max}$) that the electromagnetic wave can run before the next pulse is transmitted. In formulas $r_{\max}$ can be expressed as follows:

$$r_{\max} = \frac{c}{2\text{PRF}}, \tag{1.2.1}$$

where c (m/s) indicates the light velocity and the factor 2 is due to the two-way trip (from the antenna to the target and from the target to the antenna) of the transmitted pulses.

While the PRF limits the maximum detectable range $r_{\max}$, the time duration of the pulses T_0 limits the radial horizontal spatial resolution Δr (see Fig. I.2.1), i.e., targets separated in space by at least Δr will be completely resolved in range. Consider two targets located at ranges r_1 and r_2, with $r_1 < r_2$. The signals corresponding to these targets, after sending a pulse, will be received, respectively, at the instants t_1 and t_2. Then, the distance between the targets $\Delta r_t = (r_2 - r_1)$ can be computed as $\Delta r_t = c(t_2 - t_1)$. If the two targets are at least of $cT_0/2$ apart, the trailing edge of the received pulse from the first target is well separated (i.e., it is not overlapped) to the leading edge of the received pulse from the second target. Therefore, the radial horizontal spatial resolution of radar is given by

$$\Delta r = \frac{cT_0}{2}. \tag{1.2.2}$$

In the latter, Δr is expressed in meters when T_0 in seconds and c in meter·per second.

The receiver detects the radar signal, amplifies it, converts from analog to digital, and averages the returned pulses over defined time periods. If the observed target is moving, the received signal shows a Doppler frequency shift f_0 which can be detected by the coherent receiver (see blocks after the IF amplifier on Fig. I.2.1). The in-phase (I) and the in-quadrature (Q) components at the output signal of the coherent receiver are then used to retrieve the Doppler velocity of the observed target. Typical peak transmitted power is 10^5–10^6 W, whereas typical received power is 10^{-10} W. The circulator protects the sensitive receiver from the powerful transmitter.

Eventually, radar antennas focus the transmitted energy and direct it along a narrow angular beam. For scanning radars (i.e., radars that are able to roundly move its antenna for several elevation angles), this direction is often described in terms of an elevation angle relative to the ground and an azimuth angle relative to the north. The radar energy is higher along the center of the beam and decreases outward with increasing angular width. The beam width is defined as the angular width where the power is exactly half the maximum power (or –3 in dB scale). Along the vertical and horizontal directions these angles are, respectively, labeled as $\Theta_{3\text{dB}}$, $\Phi_{3\text{dB}}$. Then the resolution volume ΔV (m^3), illuminated by a transmitted pulse along the beam, is approximated by a cylinder as shown in Fig. I.2.1. Therefore, the volume of this cylinder can be expressed as follows:

$$\Delta V = \Delta r \cdot \Delta S \cong \left(\frac{cT_0}{2}\right)\left(\frac{r\Theta_{3\text{dB}}}{2}\right)\left(\frac{r\Phi_{3\text{db}}}{2}\right)\pi = \frac{cT_0\Theta_{3\text{dB}}\Phi_{3\text{db}}}{8}\pi r^2. \quad (1.2.3)$$

As can be observed from the latter expression, the resolution volume becomes more and more large as the distance from the radar increases.

Last consideration concerns the polarimetric radar schemes where both the transmission and receiver sections are, in some way, replicated to, respectively, transmit and receive the horizontal and vertical polarized waves. Indeed, either alternate dual-polarization schemes (with a suitable switch) or a hybrid slant linear polarization transmitting scheme can be used, the latter being nowadays the most applied.

2.2 Radar Equation for Single Target

The radar equation expresses the relationship between the transmitted power (W_t) and the backscattered received power (W_r) from precipitation targets in terms of the radar's hardware characteristics and the distance between the transmitter and the target.

Let us consider a single target, shown in Fig. I.2.2, at distance r from the radar. The incident power density (P_i) on the target, expressed in W/m^2, is given by the

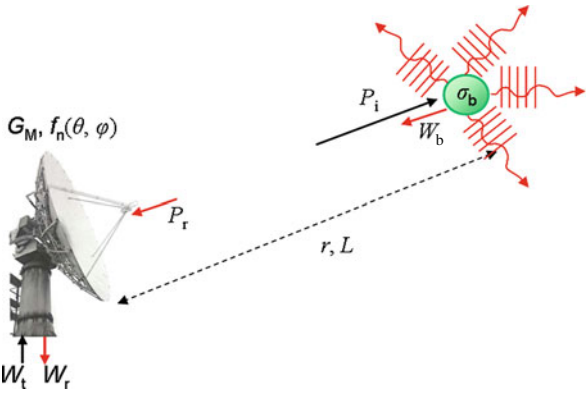

Fig. I.2.2 Transmission and reception of radar pulses from a single target. W_r, received power; W_t, transmitted power; P_r, received power density; P_i, incident power density on the target; W_b, radar backscattered power from the target; G_M, maximum antenna gain; f_n, normalized antenna radiation pattern; σ_b, radar backscattering cross section

power, distributed over a sphere or ray r, weighted by the antenna gain G which reassumes the antenna radiation efficiency and its directive properties:

$$P_i(r, \theta, \varphi) = \frac{W_t}{4\pi r^2} G(\theta, \varphi) L(r). \tag{1.2.4}$$

In Eq. (1.2.4) $L(r)$ is the loss factor of the medium which separates the target from the antenna, θ and φ are, respectively, the antenna elevation and the azimuth angle. $G(\theta, \varphi)$ can be split up, for convenience, into two terms as follows:

$$G(\theta, \varphi) = G_M \cdot |f_n(\theta, \varphi)|^2 , \tag{1.2.5}$$

where G_M represents the maximum antenna gain, whereas f_n accounts only for the directional properties of the antenna. After interacting with the target, the incident wave is partially scattered back to the radar. More in detail, when an electromagnetic wave hits on a dielectric particle, both scattering and absorption contribute to the loss of energy of the incident wave. The absorption causes the loss of power from the incident wave since the power is absorbed by the target and dissipated as heat. On the other hand, the scattering diffuses the incident power in many directions and the loss of energy manifests when these directions are those undesired with respect to the location of the transmitter and the receiver. The combination of the absorption and scattering is called extinction of the electromagnetic wave. The extinction can be described by the radar cross section or also called extinction cross section (σ_e) usually expressed in square meter. It can be defined as the ratio between the resulting power after the extinction of the wave (W_e) and the incident power density (P_i). Obviously σ_e is a function of the direction through the angles θ and φ. If the line of sight between the radar and the target is considered, only the backscattered power (W_b) has to be accounted for the computation of the received power W_r. Therefore the backscattering radar cross section ($\sigma_b = W_b/P_i$), instead of σ_e, will be used in

the next formulas. With the definition of σ_b in mind, the received power density (P_r) at the radar antenna aperture is given by

$$P_r(r,\theta,\varphi) = \frac{P_i(r,\theta,\varphi)\cdot\sigma_b}{4\pi r^2}\cdot L(r). \tag{1.2.6}$$

The received power (W_r) can be obtained exploiting the characteristic of a receiving antenna to transform the intercepted power density at its aperture into a power at its output. This characteristic is the antenna equivalent area (A_e). For whatever antenna (Balanis, 1997) the following holds:

$$A_e(\theta,\varphi) = \frac{\lambda^2}{4\pi}\cdot G(\theta,\varphi). \tag{1.2.7}$$

The received power can be then expressed as follows:

$$W_r = P_r(r,\theta,\varphi)\cdot A_e(\theta,\varphi). \tag{1.2.8}$$

Substituting Eq. (1.2.4) in Eq. (1.2.6) and using both Eqs. (1.2.7) and (1.2.8) for the expressions of A_e and G, the received power can be explicated as indicated below:

$$W_r = \underbrace{\left(\frac{W_t G_M^2\,|f_n(\theta,\varphi)|^4\,\lambda^2}{(4\pi)^3}\right)}_{c_1}\cdot L^2\cdot\frac{\sigma_b}{r^4} = C_1\cdot L^2\cdot\frac{\sigma_b}{r^4}. \tag{1.2.9}$$

In the latter expression the radar constant C_1 has been introduced. This is made possible since the single target is supposed to be perfectly enclosed in the main lobe of the antenna along the direction of maximum radiation where $f_n = 1$.

2.3 Radar Equation for Distributed Target

Precipitation particles, such as raindrops, snowflakes, hail, and graupel, act as distributed scatters in the volume of the atmosphere illuminated by the precipitation radar. The backscattered signal from a volume of randomly distributed targets is the sum of the signals scattered by each of the single target within that volume. It is suitably defined as a quantity called radar reflectivity for unit volume, that is,

$$\eta = \frac{\sum_i \langle\sigma_{bi}\rangle}{\Delta V}, \tag{1.2.10}$$

where the summation is extended to all the radar backscatter cross sections σ_{bi} of the particles within the radar resolution volume ΔV (m^3), which is specified in Eq. (1.2.3), and "<·>" is the time average operator that considers all the received samples in a given time interval. Considering all the terms which depend on the

position within the resolution volume in Eq. (1.2.9) and weighting them with the antenna gain function $G(\theta, \varphi)$, the average received power assumes the following form:

$$\langle W_r \rangle = \frac{W_t \lambda^2}{(4\pi)^3} L^2 \int_{\Delta V} \frac{G^2(\theta, \varphi)}{r^4} \eta dV \tag{1.2.11}$$

Exploiting again Eq. (1.2.9) for expressing the antenna gain function $G(\theta, \varphi)$ and expressing the infinitesimal element of volume dV equals to $r^2 \cdot dr \cdot d\Omega$ and dr as $cT_0/2$ as in Eq. (1.2.2), Eq. (1.2.11) becomes

$$\langle W_r \rangle \cong \frac{W_t \lambda^2 G_M^2}{(4\pi)^3} \left(\frac{c}{2} T_0\right) \frac{\eta}{r^2} L^2 \int_{\Omega} |f_n(\theta, \varphi)|^4 d\Omega \tag{1.2.12}$$

Assuming a Gaussian function for describing the radiation pattern f_n of the radar antenna, the integral in Eq. (1.2.12) can be approximated (Probert-Jones, 1962) as written below:

$$\int_{\Omega} |f_n(\theta, \varphi)|^4 d\Omega \cong \frac{\pi \Theta_{3dB} \Phi_{3dB}}{8 \ln 2} \tag{1.2.13}$$

Substituting Eq. (1.2.13) in Eq. (1.2.12), the average received power, in its final form, assumes the following expression:

$$\langle W_r \rangle \cong \underbrace{\left(\frac{W_t G_M^2 \lambda^2 c T_0 \Theta_{3dB} \Phi_{3dB}}{1024 \cdot \ln 2 \cdot (\pi)^2} \right)}_{C_2} \cdot L^2 \cdot \frac{\eta}{r^2} = C_2 L^2 \frac{\eta}{r^2} \tag{1.2.14}$$

As in the case of the single target, the radar calibration constant (C_2) includes all the dependencies from the hardware specifications. We observe that the dependence of W_r is now on r^{-2} instead of r^{-4} as for single target equation but this is simply the consequence of the integration of all the distributed targets. The knowledge of the constant C_2 and the measure of W_r allows the retrieving of the reflectivity for unit volume η. The constant C_2 is calculated through a calibration process, for example, measuring the power received by a target of known radar reflectivity. Typical lower bounds for C_2 are 0.5–1 dB. In the next section, the average power <Wr> will be expressed as a function of the widely used radar reflectivity factor instead of the radar reflectivity for unit volume as done in Eq. (1.2.14) (Fig. I.2.3).

2.3.1 Microwave Backscattering Models

To be valuable in precipitation studies, the average returned power, measured by weather radars, expressed by Eq. (1.2.14), must be related to the physical characteristics of the precipitation particles within the radar resolution volume. To pursue

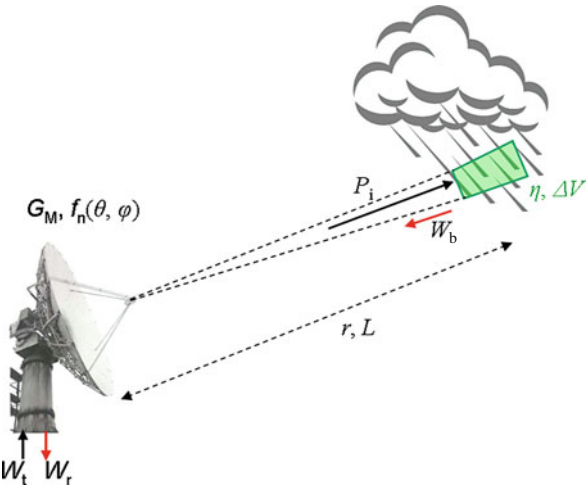

Fig. I.2.3 Transmission and reception of radar pulses from a distributed target. W_r, received power; W_t, transmitted power; P_i, incident power density on the target; η, volumetric reflectivity; ΔV, radar resolution volume; G_M, maximum antenna gain; f_n, normalized antenna radiation pattern

this aim and to maintain the treatment also valid for polarimetric radars, in the next sections, the polarimetric radar principles will be introduced and expressions of the reflectivity will be derived for the spherical particles in the Rayleigh and the Mie approximations, i.e., respectively, the case where the wavelength of the transmitted signal is much larger than the geometrical cross section of the target and the opposite situation. The case of non-spherical particles will be discussed as well.

2.4 Radar Polarimetry

It is well established (Jones, 1959; Pruppacher and Beard, 1970; Pruppacher and Pitter, 1971; Bringi et al., 1998) that small raindrops (i.e., with diameter less than 1 mm) are spherical, whereas larger raindrops are deformed by aerodynamic forces into horizontally oriented oblate spheroids. An oblate spheroid is the body of revolution formed when an ellipse with minor axis dimension (a) and major axis dimension (b) is rotated about its minor axis. Raindrops usually fall with their maximum dimension oriented horizontally. This orientation may be temporarily disturbed by turbulence, drop collision, or aerodynamic instability. The differences in the ratio between the horizontal and vertical dimensions of larger drops result in different electromagnetic properties of the scattered energy when the incident energy is horizontally versus vertically polarized. A special type of precipitation radar, called polarimetric radar, is designed to measure these properties by transmitting and receiving radiation in more than one orientation. Ongoing research (e.g., Gorgucci et al., 2000; Vivekanandan et al., 2004; Marzano et al., 2008) has shown that polarization radar variables involving the differential amplitude and phase of the received power at orthogonal polarizations can be related to the physical characteristics of the precipitation. Among others, two commonly used polarimetric variables in precipitation applications are the differential reflectivity (Z_{dr}), related to the axis

ratio of the precipitation particles and specific differential propagation phase shift (K_{dp}), related to liquid water content. These radar observables and the polarimetric radar principles will be introduced in the next sections.

2.4.1 The Polarization State

The polarization of the radiated wave, which is coincident by definition with the antenna polarization, is defined as "that property of an electromagnetic wave describing the time varying direction and relative magnitude of the electric field vector (**E**); specifically the figure traced as a function of time by the extremity of the vector **E** at a fixed location in space and the sense in which it is traced, as observed by the along the direction of propagation" (Balanis, 1997).

Polarization then is the curve traced by the end point of the arrow representing the instantaneous electric field. The field must be observed along the direction of propagation. A typical trace as a function of time is shown in Fig. I.2.4. The polarization of a field is generally elliptic that is the arrow representing the instantaneous electric field describes an ellipse as indicated in panel (b) of Fig. I.2.4. Special cases of the elliptical polarization are the circular polarization, which occurs when the major (OA) and minor (OB) axes of the ellipse coincide and the linear polarization which is the degeneration of the ellipse in a line.

2.4.2 The Scattering Matrix

Before describing the scattering of a plane electromagnetic wave by a drop and more in general by a non-spherical particle in an arbitrary orientation, it is necessary to

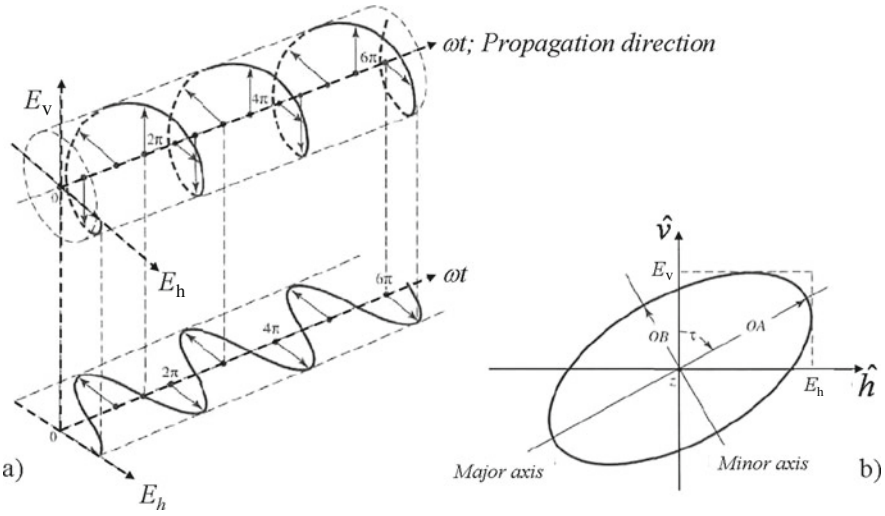

Fig. I.2.4 Rotation of a plane electromagnetic wave (panel **a**) and its polarization ellipse, at ωt=0 (panel **b**), as a function of time (Balanis, 1997)

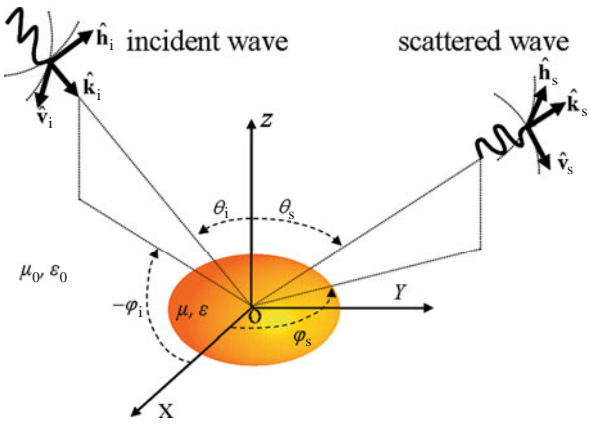

Fig. I.2.5 FSA convection for representing incident and scattered waves

specify the directions of the incident and the scattered waves and the orientation of the particle with respect to a reference frame.

In this section the concepts of polarization and the scattering from a single particle will be introduced. Following the notation used in Zly and Ulaby reported in Bringi and Chandrasekar (2001), consider a particle positioned at the origin of a Cartesian reference system as shown in Fig. I.2.5. The direction of incidence (i) of the plane wave is specified by the angles θ_i and φ_i or alternatively by the triplet $\hat{k}_i$, $\hat{h}_i$, $\hat{v}_i$ shown in the same figure, where h and v define the plane where the incident electric field ($\mathbf{E}_i$) varies. With this notation in mind the electric field vector can be formulated as follows:

$$\mathbf{E}^i(O) = E_i^h \hat{h}_i + E_E^v \hat{v}_i \Rightarrow \mathbf{E}^i(O) = \begin{bmatrix} E_i^h \\ E_i^v \end{bmatrix} \tag{1.2.15}$$

In Eq. (1.2.15) $\mathbf{E}_i$ has been expressed as a function of the two components, respectively, along the horizontal (E_i^h) and vertical (E_i^v) directions. The directions h and v assume a useful descriptive significance when $\theta_i \approx 90°$ and the plane XY becomes the Earth's surface and k_i is parallel on it. In order to express the scattered electric field ($\mathbf{E}_s$), a reference system analogous to that just introduced for the incident wave can be used. Then, the vector $\mathbf{E}_s$ can be described by the triplet $\hat{k}_s, \hat{h}_s, \hat{v}_s$ as shown in Fig. I.2.5.

The geometrical convention just introduced is called forward scattering alignment (FSA) as opposed to the backward scattering alignment (BSA), where the scattered field is seen from an observer positioned at the location of the receiver antenna (and not inside the particle as in the FSA convention). However, BSA is simply formulated from FSA just considering $\mathbf{k}_r = -\mathbf{k}_s$, $\mathbf{v}_r = \mathbf{v}_s$, and $\mathbf{h}_r = -\mathbf{h}_s$, where the subscript "r" indicates the received wave from the radar.

When a plane wave hits a particle, in it, an electrical field ($\mathbf{E}_{int}$) is generated. $\mathbf{E}_{int}$ can be considered as the source of the scattered field ($\mathbf{E}_s$) from the particle. The exact formulation of the scattered field can be obtained solving the Helmholtz

equation which is directly derived from the Maxwell ones. At great distance from the spherical particle of dielectric constant ε_r the following expression holds:

$$\begin{aligned}\mathbf{E}_s(\mathbf{k}_s) &= \frac{k_0^2}{4\pi}(\varepsilon_r - 1)\frac{e^{-jk_0 r}}{r}\int_V \left[\mathbf{E}_{int}^T(\mathbf{k}) - \hat{k}_s\left(\hat{k}_s \cdot \mathbf{E}_{int}^T\right)\right] e^{jk_0 \cdot \mathbf{k} \cdot \mathbf{k}_s} d\tau \\ &= \frac{e^{-jk_0 r}}{r} \cdot \mathbf{f}\left(\hat{k}_i,\ \hat{k}_s\right),\end{aligned} \tag{1.2.16}$$

where r is the distance between the particle and an observation point in the free space, V the volume of the particle, k_0 the propagation constant in the free space, and $\mathbf{f}$, in the third term of Eq. (1.2.16), the complex scattering amplitude function which describes the scattering properties of the considered particle.

The solution of the scattering problem reduces to the computation of the function $\mathbf{f}$ from the knowledge of the induced internal field $\mathbf{E}_{int}$. If $\mathbf{E}_s$ is expressed in the same form of the incident field in Eq. (1.2.15) in terms of their horizontal and vertical components, Eq. (1.2.16) can be expressed by means of the scattering matrix ($\mathbf{S}$). The scattering matrix accounts for the scattering properties of a single particle. Using the FSA convection the scattered field is linked to the incident one, through $\mathbf{S}$, as follows:

$$\mathbf{E}_s = \frac{e^{-jk_0 r}}{r} \cdot \mathbf{S}_{FSA} \cdot \mathbf{E}_i \Rightarrow \begin{bmatrix} E_h^s \\ E_v^s \end{bmatrix} = \frac{e^{-jk_0 r}}{r} \cdot \begin{bmatrix} S_{hh} & S_{hv} \\ S_{vh} & S_{vv} \end{bmatrix}_{FSA} \cdot \begin{bmatrix} E_h^i \\ E_v^i \end{bmatrix} \tag{1.2.17}$$

where h and v represent the horizontal and vertical polarizations for the transmitted (given by the second subscript) and received (given by the first subscript) signals. The FSA convection is oriented to give more importance to the direction of propagation of the scattered wave. For radar applications the BSA convection is used instead of the FSA one. According to BSA, the received electrical field can be expressed as follows:

$$\mathbf{E}_r = \frac{e^{-jk_0 r}}{r} \cdot \mathbf{S}_{BSA} \cdot \mathbf{E}_i \Rightarrow \begin{bmatrix} E_h^r \\ E_v^r \end{bmatrix} = \frac{e^{-jk_0 r}}{r} \cdot \begin{bmatrix} -1 & 0 \\ 0 & 1 \end{bmatrix} \cdot \begin{bmatrix} S_{hh} & S_{hv} \\ S_{vh} & S_{vv} \end{bmatrix}_{FSA} \cdot \begin{bmatrix} E_h^i \\ E_v^i \end{bmatrix} \tag{1.2.18}$$

It is worth mentioning that the scattering matrix elements depend on the directions of incidence and scattering of the electromagnetic wave as well as on the size, morphology, and composition of the particle. In general, it seems reasonable to find a connection between the scattering matrix elements and the radar cross section of the particle seen from the radar from different polarizations. Indeed, this relationship exists and is reported here (see Bringi and Chandrasekar, 2001 for details):

$$\sigma_{ij} = 4\pi \left|S_{ij}\right|^2 \tag{1.2.19}$$

where the indexes "i" and "j" indicate all the possible combinations of the polarizations h and v and S_{ij} are the elements of the scattering matrix $\mathbf{S}$. For monostatic

radars (i.e., radars where one single antenna transmits and receives signals), the reciprocity theorem is valid and the cross-polarization elements of the scattering matrix are identical:

$$(S_{\mathrm{hv}} = S_{\mathrm{vh}})_{\mathrm{BSA}} \tag{1.2.20}$$

For spherical particles the radar sees the same section whatever polarization h of v is used, then the following two relations hold:

$$S_{\mathrm{hh}} = S_{\mathrm{vv}} = S_{\mathrm{sphere}} \tag{1.2.21}$$

and

$$S_{\mathrm{hv}} = S_{\mathrm{vh}} = 0 \tag{1.2.22}$$

The analytical expression for S_{sphere} will be shown in the next section.

For non-spherical drops S_{hh} and S_{vv} will not be equal and, furthermore S_{hv} and S_{vh} will not be 0. However, if we assume that every single raindrop is uniformly oriented with zero canting angle (i.e., with their axes of symmetry vertically aligned with respect to the direction of incidence of the transmitted radar signal), S_{hv} and S_{vh} continue to be 0.

2.5 Scattering from Spherical Particles

In this section the expression of the received average power ,Wr> formalized in Eq. (1.2.14) will be further developed by better specifying the expression of the volume radar reflectivity η. If the radar volume is filled by some particles with a distribution $N(D)$ and equivalent diameter D, Eq. (1.2.10) that represents the sum of the radar backscattering cross section σ_{bi} of individual particles over unit volume can be extended as follows:

$$\eta = \frac{\sum_i \sigma_{\mathrm{b}i}}{\Delta V} = \int_0^\infty \sigma_{\mathrm{b}}(D) N(D) dD, \tag{1.2.23}$$

where $N(D)$ is expressed in $\mathrm{mm}^{-1}\cdot\mathrm{m}^{-3}$, the radar backscattering cross section σ_{b} in square meter, and D in millimeter. The radar reflectivity characterizes the target properties and its definition is independent from the nature of the scattering medium. If $D/2 << \lambda$ (it is often assumed in equivalent manner D less than $\sim\lambda/16$), the expression of the backscattering cross section, for a spherical particle, assumes a simple form as follows:

$$\sigma_{\mathrm{b}} = \frac{k_0^4}{4\pi} \cdot \left| \frac{3 \cdot (\varepsilon_{\mathrm{r}} - 1)}{\varepsilon_{\mathrm{r}} + 2} \right|^2 \cdot V_{\mathrm{Sphere}}^2 = \frac{\pi^5}{\lambda^4} \cdot |K_l|^2 \cdot D^6 \tag{1.2.24}$$

where $V_{\text{sphere}} = (\pi/6) \cdot D^3$ is the volume of the equivalent sphere, $k_0 = 2\pi/\lambda$ is the propagation constant in the free space, and $|K_l|^2 = |(\varepsilon_r - 1)/(\varepsilon_r + 2)|^2$ is a quantity called dielectric factor of the microphysical species "l" (e.g., $l = w$ for water and $l = i$ for ice) which depends on wavelength (λ), temperature, and dielectric constant (ε_r). $|K_l|^2$ can assume different values such as $|K_w|^2 = 0.93$ for water and for temperatures in the range 0–20°C and $|K_i|^2 = 0.208$ for ice with density of about 1 g/m^3.

Equation (1.2.24) is referred to as the Rayleigh approximation of the backscattering cross section. Under the Rayleigh regime, the normalized radar cross section, with respect to the geometrical cross section (also called backscattering efficiency ξ_b), increases as the fourth power of the ratio D/λ (see Fig. I.2.6 in logarithm coordinates). When the equivalent diameter is greater than $\sim\lambda/16$ Mie or optical scattering occurs. In contrast to Rayleigh scattering, under conditions of Mie scattering, the backscattered returned power fluctuates as the size of the scatter increases. This phenomenon is shown in Fig. I.2.6.

Following the Rayleigh theory and substituting Eq. (1.2.24) in Eq. (1.2.23), an expression of the volumetric reflectivity as a function of size distribution of diameters, dielectric properties, particle sizes, and the radar frequency is obtained and is made explicit here in the following equation:

$$\eta = \frac{\pi^5}{\lambda^4}|K_l|^2 \cdot \underbrace{\int_0^\infty D^6 \cdot N(D)dD}_{z} = \frac{\pi^5}{\lambda^4}|K_l|^2 \cdot Z, \tag{1.2.30}$$

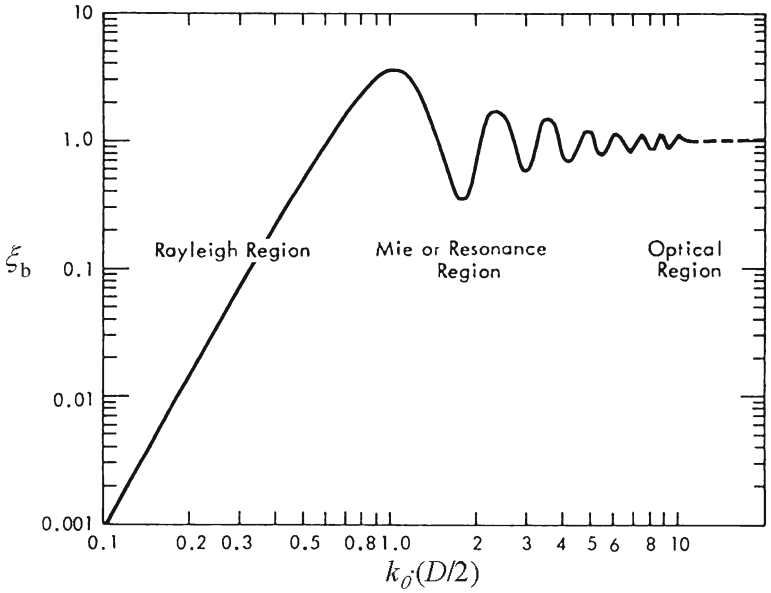

Fig. I.2.6 Backscattering efficiency $\xi_b = \sigma_b \cdot \left[\pi(D/2)^2\right]^{-1}$ as a function of $k_0 \cdot D/2$ for different backscattering regimes

where Z is the radar reflectivity factor (it should not be confused with the radar reflectivity for unit of volume η) expressed in mm^6/m^3 and as can be observed from Eq. (1.2.30), under Rayleigh approximation, it coincides with the statistical moment of order six of the size distribution of rainy drops.

Similarly to η, the reflectivity factor Z can be also interpreted as an average characteristic of the population of scatters distributed in a given radar volume. Z is independent from the wavelength and this property makes easier the comparison of reflectivity factors derived from different radar systems.

If the Rayleigh condition is not satisfied and Mie scattering holds, an equivalent reflectivity factor, Z_e, is conveniently introduced and the third term of Eq. (1.2.30) is still valid when Z_e instead of Z is considered and $l{=}w$, indicating a dielectric factor K referred to water. Z_e can be interpreted as the reflectivity factor of a population of liquid and spherical particles satisfying the Rayleigh approximation and producing a signal of the same power produced by a generic set of targets within the radar volume. Thus, in the Mie scattering Z_e is given by

$$Z_e = \frac{\lambda^4}{\pi^4 \cdot |K_w|^2} \cdot \eta \tag{1.2.31}$$

With Eqs. (1.2.30) and (1.2.31) in mind, the average power received by a radar in Eq. (1.2.14) can be updated and, in general, it depends, among other parameters, on the equivalent radar reflectivity and then on the physical characteristics of the observed particles. It is important to note that Z describes the characteristics of the target in a way independent of the wavelength. In addition, in the case of spherical particles, as discussed before the scattering matrix is completely defined through the expression of the radar cross section.

2.6 Scattering from Spheroidal Particles

The solution of the scattering and absorption problems of the electromagnetic waves from dielectric spheres with arbitrary size has been obtained by Mie in 1908 (Ulaby et al., 1986). The Mie solution is well known and it has been used for studying a lot of physical systems. However, various problems, such as the interaction of the electromagnetic waves with the hydrometeors, are related to the scattering from non-spherical bodies at wavelength comparable with the size of the observed particles. The extended boundary condition method (EBCM) also called T-matrix method (where "T" stands for transition) provides the solution of this class of problems and allows the computation of the scattering matrix through a numerical implementation. This technique was initially introduced by Waterman (1971) as a technique for computing electromagnetic scattering by single, homogeneous, arbitrarily shaped particles based on the Huygens principle. An important feature of the T-matrix approach is that it reduces exactly to the Mie theory when the scattering particle is a homogeneous or layered sphere composed of isotropic materials. Even though the T-matrix is potentially applicable to arbitrarily shaped particles, most of the

implementation refers to the computation of the scattered field for revolution solids such as cones, cylinders, and spheroids (Mishchenko and Travis, 1998).

More in detail, the aim of this method is to compute the scattered field from an arbitrarily shaped particle when it is illuminated by an incident plane wave. The field in every point of the space is given from the sum of the incident wave and the scattered one, where the incident wave is considered without the presence of the particle. The scattered field can be thought to be generated from superficial currents which have been induced on the particle by the incident wave. Then the T-matrix determinates the scattered field as a function of the incident field and the physical characteristics of the particle. This can be obtained by applying the equivalence theorem (of Love) in which the scattered field is assumed generated by some induced superficial currents which are supposed to be localized on the extreme surface of the particle. The core of the procedure consists of the following steps:

1. Relate the field internal to the particle to the external one
2. Determinate the superficial currents as a function of the internal field found at the previous step
3. Compute the scattered field generated by the superficial currents

Without considering all the mathematical passages, in formulas, the T-matrix approach expresses both the incident and the scattered fields as a linear combination of vectorial functions of the spheric waves which are solutions of the vectorial Helmholtz equation. These functions, indicated as $\mathbf{M}_{nm}$ and $\mathbf{N}_{mn}$ are called multipole. Therefore, an incident electric field polarized along the x-direction and propagating along the z-direction is expressed as follows:

$$\underline{\mathbf{E}}^i = \hat{x} E_0 e^{-jk_0 z} = \sum_{n=1}^{\infty} [a_{\mathrm{o}1n} \cdot \mathbf{M}_{\mathrm{o}1n}(k_0 r,\ \theta,\ \varphi) + b_{\mathrm{e}1n} \cdot \mathbf{N}_{\mathrm{e}1n}(k_0 r, \theta, \varphi)], \quad (1.2.32)$$

where a_{01n} and b_{01n} are known coefficients. The same expansion can be done for the scattered field in terms of the unknown coefficients f_{01n} and g_{01n}:

$$\underline{\mathbf{E}}^s = \sum_{n=1}^{\infty} \left[f_{\mathrm{o}1n} \cdot \mathbf{M}_{\mathrm{o}1n}(k_0 r,\ \theta,\ \varphi) + g_{\mathrm{e}1n} \cdot \mathbf{N}_{\mathrm{e}1n}(k_0 r, \theta, \varphi) \right] \quad (1.2.33)$$

Due to the linearity of the Maxwell's equations and boundary conditions, the relation between the scattered field coefficients (f_{01n} and g_{01n}) and the incident field coefficients (a_{01n} and b_{01n}) must be linear and is given by the transition matrix T (or T-matrix) (Waterman, 1971; Mishchenko, 2000):

$$\begin{bmatrix} f_{\mathrm{o}1n} \\ g_{\mathrm{e}1n} \end{bmatrix} = \underbrace{\begin{bmatrix} T^{11} & T^{12} \\ T^{21} & T^{22} \end{bmatrix}}_{T} \times \begin{bmatrix} a_{\mathrm{o}1n} \\ b_{\mathrm{e}1n} \end{bmatrix} \quad (1.2.34)$$

Once the T-matrix for a given particle is known, Eq. (1.2.33) can be used to determine the scattered field and then to derive the scattering matrix introduced before. The T-matrix, which is completely independent of the propagation directions and polarization states of the incident and scattered fields, depends only on the scattering particle characteristics (size relative to the wavelength, shape, relative refractive index, and orientation with respect to the laboratory reference frame). This means that for any particular particle, the T-matrix only needs to be calculated once and can then be used for repeated calculations. This is a significant advantage over many other methods of calculating scattering where the entire calculation needs to be repeated.

2.7 Radar Observables

In this section a review of the main radar observables is exposed. For major details about these observables refer to Bringi and Chandrasekar (2001). References about algorithms that use polarimetric radar observables for rain estimation can be found in Chandrasekar and Bringi (1987), Testud et al. (2000) and Ryzhkov et al. (2005). For the attenuation correction problem see for example Bringi et al. (2001), Vulpiani et al. (2005).

2.7.1 Reflectivity Factor

As mentioned before the reflectivity factor depends, in general, on the size distribution of hydrometeors, the backscattering cross section, and its physical characteristics. Since the radar signals can be received in the vertical or horizontal polarization it is opportune to refer to the co-polar reflectivity factor, expressed in Eq. (1.2.31), as follows:

$$\begin{aligned} Z_{\mathrm{e\,hh,vv}} = Z_{\mathrm{hh,vv}} &= \frac{\lambda^4}{\pi^5 |K|^2} \eta_{\mathrm{hh,vv}} = \frac{\lambda^4}{\pi^5 |K|^2} \int_{D_{\min}}^{D_{\max}} \sigma_{\mathrm{b,hh,vv}}(D) \cdot N(D) \cdot dD \\ &= \frac{4\lambda^4}{\pi^4 |K|^2} \left\langle |S_{\mathrm{hh,vv}}|^2 \right\rangle \end{aligned} \tag{1.2.35}$$

where $D_{\min}$ and $D_{\max}$ are the minimum and maximum particle diameters, $S_{\mathrm{hh,vv}}$ are the backscattering co-polar components of the scattering matrix **S** at horizontal and vertical polarizations, respectively, $|K|^2 = |(\varepsilon_{\mathrm{r}} - 1)/(\varepsilon_{\mathrm{r}} + 2)|^2$ is the complex dielectric constant of scattering particle which is a function of wavelength and temperature, and the operator "<·>" indicates the ensemble average over the drop size distribution. In the fourth term of Eq. (1.2.35), Eq. (1.2.24) has been used. The reflectivity factor has the unit of $\mathrm{mm}^6 \cdot \mathrm{m}^{-3}$ but it is often expressed in decibels of Z (dBZ) defined as $10 \log_{10}(Z_{\mathrm{ehh,vv}})$. Henceforth, for simplifying the notation, the equivalent reflectivity factor Z_{e} will be indicated as Z.

2.7.2 Differential Reflectivity

Among the main important observables of polarimetric radars, the differential reflectivity Z_{dr} plays a relevant role. To obtain radar reflectivity, energy is transmitted and received at the same polarization, usually horizontal. Differential reflectivity is the difference between the horizontally transmitted and horizontally received reflectivity factor (Z_{hh}) and the vertically transmitted and vertically received reflectivity factor (Z_{vv}). This is expressed, in logarithmic scale, in the following equation:

$$Z_{dr} = 10 \cdot \log_{10} \frac{Z_{hh}}{Z_{vv}} = 10 \cdot \log_{10} \frac{\langle |S_{hh}|^2 \rangle}{\langle |S_{vv}|^2 \rangle} \tag{1.2.36}$$

Differential reflectivity is a measure of the reflectivity-weighted mean axis ratio (a/b) of precipitation particles in a resolution volume. Z_{dr} depends on the shape and on the common orientation degree but it is independent from the number of particles in the radar volume. The measurement process of Z_{dr} can be obtained alternatively transmitting and receiving h and v in linear polarization. These measurements should be made very fast with respect to the time variation of the target geometry or in other words within the correlation time of the received time series.

Differential reflectivity has many potential applications, such as rainfall estimation, discrimination between liquid and frozen precipitation, and detection of biological scatterers (Zrnic, and Ryzhkov, 1998). For rain, as raindrops increase in volume, the drop diameter D increases, the shape of the drop becomes more oblate, the axis ratio decreases, and the associated Z_{dr} value increases. For spherical drops or spherical ice particles, the axis ratio a/b approximates the unity and $Z_{dr} \approx 0$. Table I.2.1 summarizes typical ranges of differential reflectivity values for several types of precipitations.

For ideal radar systems, differential reflectivity, being the ratio of reflectivity at horizontal and vertical polarizations, would not be affected by radar calibration errors. Nevertheless, because of unequal paths or gains in the horizontal- and vertical-polarized channels of the radar receiver, Z_{dr} can be biased. When viewed vertically, raindrops of all sizes appear circular and have an associated Z_{dr} value equal to 0. Thus, a Z_{dr} bias, accounting for the relative difference in calibration

Table I.2.1 Typical ranges of observed differential reflectivity values for several types of precipitations between S and X bands

Z_{dr} (dB)	Associated precipitation types
<–0.5	Marginally detectable precipitation
–0.5 to 0.5	Drizzle, very light rain, light snow
>1	Moderate rain and heavier snow
0.5 to 4	Moderate to heavy rain
–2 to 0.5	Hail and graupel
0.5 to 4	Melting snow particles

Values adapted from Straka et. al. (2000).

between the horizontal and vertical polarizations, can be estimated by pointing the radar beam directly upward in rain.

2.7.3 Linear Depolarization Ratio

Radiowave depolarization is characterized by the presence of an anisotropic propagation medium which produces different effects (i.e., different attenuations and phase shifts) on radio waves with different polarizations. The wave will have its polarization state altered such that power is transferred (or coupled) from the desired polarization state to the undesired orthogonal polarization state, resulting in interference or crosstalk between the two orthogonally polarized channels. Hydrometeors whose principal axes are not aligned with the electrical field of the transmitted wave (see Fig. I.2.7 panel b) will cause a small amount of energy to be depolarized and to appear at the orthogonal polarization (see Fig. I.2.7 panel a). The effect is measured by the linear depolarization ratio (the term linear is used to indicate linear polarization) defined as the ratio of the cross-polar to the co-polar signals.

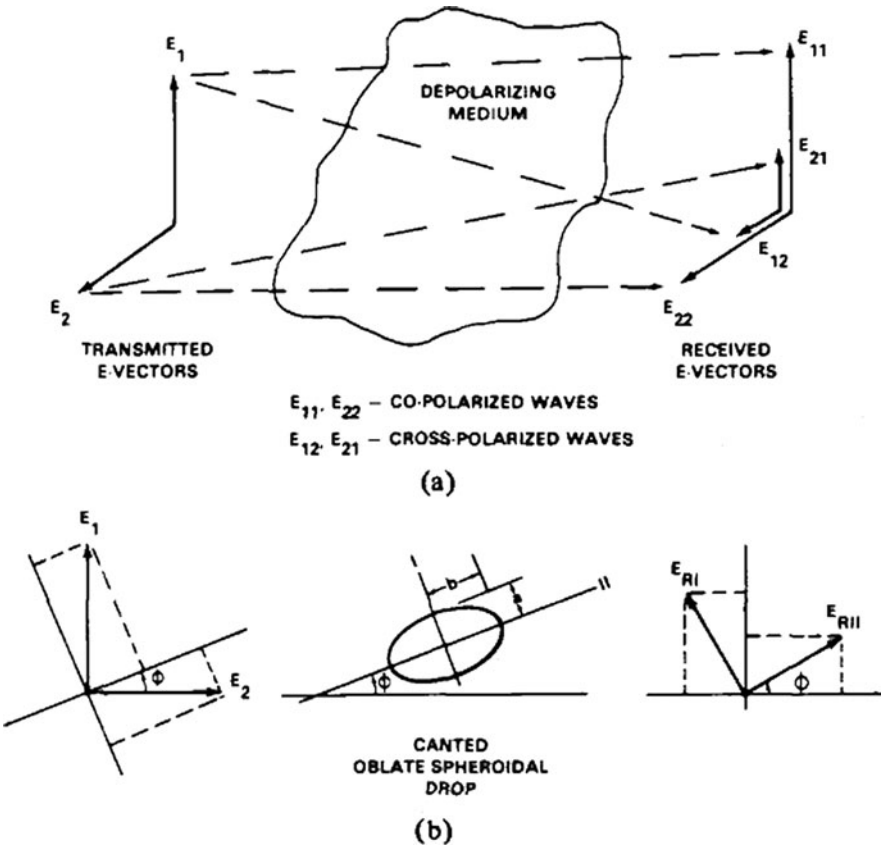

Fig. I.2.7 Vector relationships for a depolarizing medium: (**a**) co- and cross-polarized waves for linear transmission and (**b**) classical model for a canted oblate spherical rain drop

$$LDR_{\mathrm{hv}} = 10 \cdot \log_{10} \frac{Z_{\mathrm{hv}}}{Z_{\mathrm{vv}}} = 10 \cdot \log_{10} \frac{\langle |S_{\mathrm{hv}}|^2 \rangle}{\langle |S_{\mathrm{vv}}^2| \rangle}$$
$$LDR_{\mathrm{vh}} = 10 \cdot \log_{10} \frac{Z_{\mathrm{vh}}}{Z_{\mathrm{hh}}} = 10 \cdot \log_{10} \frac{\langle |S_{\mathrm{vh}}|^2 \rangle}{\langle |S_{\mathrm{hh}}|^2 \rangle}, \tag{1.2.37}$$

where the operator "<·>" indicates the ensemble average over the drop size distribution. $\mathrm{LDR_{hv}}$ and $\mathrm{LDR_{vh}}$ have similar properties because they differ only by the differential reflectivity. The depolarized signal derives from non-spheroidal particles which oscillate while falling, creating a distribution of canting angles, and from irregularly shaped particles. LDR depends on the orientation of the polarization plane of the transmitted wave, on the hydrometeors orientation, on their shape, and on their degree of common orientation.

Since LDR is a ratio between reflectivities, it is insensitive to the absolute radar calibration and to the RSD multiplicative intercept parameter. Because the cross-polar power is usually two to three orders of magnitude smaller than the co-polar signal, the linear depolarization ratio is affected by noise contamination, propagation effects, and antenna misalignments. For radars which change polarization for consecutive transmitted pulses, LDR can be contaminated by second-trip echoes. Thus, it can also be used to detect range-folded echoes. Typical values of LDR for different types of hydrometeors are listed in Table I.2.2.

2.7.4 Correlation Coefficients

The co-polar correlation coefficient is defined as

$$\rho_{\mathrm{hv}} = \frac{\int_{D_{\min}}^{D_{\max}} S_{\mathrm{vv}}(D) \cdot S_{\mathrm{hh}}^{*}(D) \cdot N(D) \cdot dD}{\sqrt{\int_{D_{\min}}^{D_{\max}} |S_{\mathrm{hh}}(D)|^2 \cdot N(D) \cdot dD \cdot} \sqrt{\int_{D_{\min}}^{D_{\max}} |S_{\mathrm{vv}}(D)|^2 \cdot N(D) \cdot dD \cdot}} = |\rho_{\mathrm{hv}}| \cdot e^{j\delta_{\mathrm{hv}}}, \tag{1.2.38}$$

where δ_{hv} (deg) is the raindrop volume backscattering differential phase shift. The magnitude is sensitive to the dispersion in particle eccentricities, canting angles,

Table I.2.2 Typical ranges of observed linear depolarization ratio values for several types of precipitations between S and X bands

LDR (dB)	Associated precipitation types
–30	Drizzle, very light rain, light snow
–25 to –30	Moderate rain and heavier snow
−15	Moderate to heavy rain
−10	Melting snow particles

Values taken from Sauvageot (1992).

irregular shapes, and the presence of mixed phase precipitation. The correlation coefficient is independent from the intercept parameter of the drop size distribution and it is insensitive to hardware calibration. Besides, it is sensitive to signal-to-noise ratio and can be contaminated by side lobes and ground clutter. Thus, it can be used to discriminate precipitation and ground clutter echoes. Radar measurements revealed that ρ_{hv} is weakly related to differential reflectivity (Balakrishnan and Zrnic, 1990; Aydin and Giridhar, 1992). As Z_{dr} increases ρ_{hv} slightly decreases.

2.7.5 Differential and Specific Differential Phase Shift

As an electromagnetic wave passes through a precipitation volume, incident energy is scattered back toward the radar and forward along the beam. The forward scattered (propagated) component of the wave becomes shifted (or in other words delayed) compared to the free space component of the wave transmitted from the radar. Within horizontally oblate raindrops, the propagating horizontal-polarized wave undergoes a larger phase shift per unit of length and travels more slowly than the vertically polarized wave. After passing through a volume filled with horizontally oblate raindrops, the horizontally polarized wave will have a larger propagation phase shift than the vertical-polarized wave. Figure I.2.8 shows a schematic interpretation of the phenomenon just exposed.

The one-way differential propagation phase (Φ_{dp}) is defined as the difference between the propagation phase shift of the horizontally transmitted and horizontally

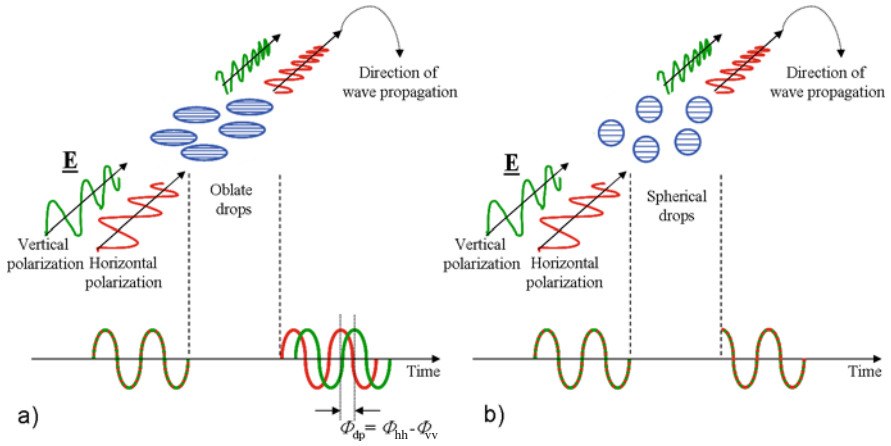

Fig. I.2.8 Schematic view of the propagation phase shift of horizontally and vertically polarized electromagnetic waves passing through a precipitation-filled volume. For simplicity the horizontally and vertically polarized waves are assumed to be in phase prior entering the volume. Panel (**a**): when the waves encounter horizontally oblate raindrops, the phase of the horizontally polarized wave is delayed more than the vertically polarized wave. Panel (**b**): when the waves encounter spherical particles such as small raindrops or hail the horizontally polarized wave and the vertically polarized wave are shifted to the same amount and $\Phi_{dp}=0$

received energy (Φ_{hh}) and the propagation phase of the vertically transmitted and vertically received energy (Φ_{vv}), that is:

$$\Phi_{dp} = \Phi_{hh} - \Phi_{vv}, \tag{1.2.39}$$

where $\Phi_{hh,vv}$ are the two-way phase angles, expressed in degrees, of the radar signal at horizontal and vertical polarizations at a particular range distance. As the radar wave passes through a region of precipitation filled with oblate drops, Φ_{dp} accumulates with increasing range. To remove range effects, Φ_{dp} is differentiated with respect to the distance from the radar "r" in order to yield the specific differential propagation phase shift (K_{dp}) which assumes the following form:

$$K_{dp} = \frac{d\Phi_{dp}}{dr}, \tag{1.2.40}$$

where K_{dp} is usually expressed in degree per kilometer.

Being K_{dp} related to the difference of phases of a plane wave propagating through a non-homogeneous medium composed of a mixture of water and air, it seems natural to relate K_{dp} to the real part of the effective propagation constant $k_{eff} = k_{\underline{eff}}^{Re} - jk_{eff}^{Im}$ (derived from the effective dielectric constant ε_{eff}).

$$K_{dp} = 10^{-3}\frac{180}{\pi} \cdot \left(k_{eff_h}^{Re} - k_{eff_v}^{Re}\right). \tag{1.2.41}$$

To highlight this aspect it is sufficient to remember that the exponential term of a plane wave which propagates, for example, along the r-direction in a medium of dielectric constant ε_{eff} is $-j \cdot k_{eff} \cdot r$ and then k_{eff}^{Re} represents a phase term, whereas k_{eff}^{Im} represents an attenuation term. Omitting all the mathematical passages [refer to Bringi and Chandrasekar (2001) for the rigorous treatment] k_{eff} assumes the following expression in the case of a slab of air with n spherical particles per unit volume:

$$k_{eff} = k_0 + \frac{2\pi n}{k_0}\hat{e}_i \cdot \underline{\boldsymbol{f}}(\hat{k}_i, \hat{k}_i) \tag{1.2.42}$$

where $\mathbf{f}$ is the vectorial scattering function introduced in Eq. (1.2.16) and $\hat{e}_i$ is the unit vector which describes the polarization of the electric field. In this case, $\mathbf{f}(\hat{k}_i, \hat{k}_i))$ describes the scattering behavior along the direction $\hat{k}_i$ in response to an incident plane wave which propagates along the same incident direction $\hat{k}_i$ (forward scattering). Substituting Eq. (1.2.42) in Eq. (1.2.41), the expression of K_{dp} for a portion of air with n particles per unit volume becomes

$$K_{dp} = 10^{-3}\frac{180}{\pi} \cdot \frac{2\pi n}{k_0}\mathrm{Re}\left[\hat{h} \cdot \underline{\boldsymbol{f}}(\hat{k}_i, \hat{k}_i) - \hat{v} \cdot \underline{\boldsymbol{f}}(\hat{k}_i, \hat{k}_i)\right] \tag{1.2.43}$$

Table I.2.3 Typical ranges of observed specific differential phase in several precipitation types

K_{dp} (deg/km)	Associated precipitation types
<–0.5	Marginally detectable precipitation
–0.5 to 0.5	Drizzle, very light rain, light snow
0.5 to 1	Moderate rain and heavier snow
0.5 to 5	Moderate to heavy rain
–0.5 to 1	Hail
–0.5 to 1	Melting snow particles

Values adapted from Straka et. al. (2000) and Bringi and Chandrasekar (2001).

In the general case, where a size distribution of particles $N(D)$ exists, Eq. (1.2.40) can be reformulated as follows:

$$K_{\mathrm{dp}} = 10^3 \frac{180}{\pi} \lambda \mathrm{Re} \left\{ \int_0^\infty N(D) \left[f_{\mathrm{hh}}(r, D) - f_{\mathrm{hh}}(r, D) \right] dD \right\}, \tag{1.2.44}$$

where the components $f_{\mathrm{hh,vv}}$ are the projection of the vectorial scattering function in the forward direction of the wave propagation $\mathbf{f}(\hat{k}_{\mathrm{i}},\ \hat{k}_{\mathrm{i}})$, along the vertical $\left(\mathbf{f}(\hat{k}_{\mathrm{i}},\ \hat{k}_{\mathrm{i}}) \cdot \hat{v}\right)$and horizontal $\left(\mathbf{f}(\hat{k}_{\mathrm{i}},\ \hat{k}_{\mathrm{i}}) \cdot \hat{h}\right)$directions.

The observable K_{dp} is not affected by electromagnetic wave attenuation since it is based on the measurement of the phase shift of the wave rather than the amplitude of the returned power. Being based on the phase shift concept, K_{dp} can be obtained when the radar beam is partially blocked as well. Beam blocking can be caused by mountainous or terrain roughness for example. In addition, K_{dp} is a very important parameter being insensitive to radar calibration, propagation effects, and system noise. Potential uses of K_{dp} include estimation of moderate and heavy rain rates, correction for attenuation losses, and verification of radar hardware calibration. Nevertheless, it is more readily contaminated by side lobe signals than the power measurements (Sachidananda, and Zrnic, 1987). A disadvantage of K_{dp} is its insensitivity to precipitation composed of small spherical raindrops, where D<1 mm and the axis ratio $a/b \approx 1$, associated with low liquid water contents and low rain rates. Typical values for K_{dp} are listed in Table I.2.3.

References

Atlas D (1954) The estimation of cloud parameters by radar. J Meteorol 11:309–317

Alberoni PP, Ferraris L, Marzano FS, Nanni S, Pelosini R, Siccardi F (2002) The Italian radar network: current status and future developments. In: Proceedings of ERAD02. pp 339–344

Aydin K, Giridhar V (1992) C-band dual-polarization radar observables in rain. J Atmos Ocean Technol 9:383–390

Balakrishnan N, Zrnic DS (1990) Use of polarization to characterize precipitation and discriminate large hail. J Atmos Sci 47:1525–1540

Balanis CA (1997) Antenna theory: analysis and design, 2nd edn. Wiley, New York, NY

Baldini L, Gorgucci E, Chandrasekar V (2004) ydrometeor classification methodology for C-band polarimetric radars. In: Proceedings of ERAD04. pp 62–66

Bringi VN, Chandrasekar V (2001) Polarimetric Doppler weather radar. Cambridge University Press, Boston, MA

Bringi VN, Chandrasekar V, Xiao R (1998) Raindrop axis ratio and size distributions in Florida rainshafts: an assessment of multiparameter radar algorithms. IEEE Trans Geosci Remote Sens 36:703–715

Bringi VN, Keenan TD, Chandrasekar V (2001) Correcting C-band radar reflectivity and differential reflectivity data for rain attenuation: a self-consistent method with constraints. IEEE Trans Geosci Remote Sens 39(9):1906–1915

Chandrasekar V, Bringi VN (1987) Simulation of radar reflectivity and surface measurements of rainfall. J Atmos Ocean Technol 4(3):464–478

Chandrasekar V, Hou A, Smith E, Bringi VN, Rutledge SA, Gorgucci E, Petersen WA, Jackson GS (2008) Potential role of dual polarization radar in the validation of satellite precipitation measurements: rationale and opportunities. Bull Am Meteorol Soc 89:1127–1145

Gorgucci E, Chandrasekar V, Bringi VN, Scarchilli G (2002) Estimation of raindrop size distribution parameters from polarimetric radar measurements. J Atmos Sci 59(15):2373–2384

Gorgucci E, Scarchilli G, Chandrasekar V, Bringi VN (2000) Measurement of mean raindrop shape from polarimetric radar observations. J Atmos Sci 57:3406–3413

Graeme LS, Vane DG, Ronald JB, Mace GG, Sassen K, Wang Z, Illingworth AJ, O'Connor EJ, Rossow WB, Durden SL, Miller SD, Austin RT, Benedetti A, Mitrescu C, the CloudSat Science Team (2002) The cloudsat mission and the A-Train, a new dimension of space-based observations of clouds and precipitation. Bull Am Meteorol Soc 83(12):1771–1790

Holleman I, Delobbe L, Anton Zgonc A (2008) The European weather radar network (OPERA): an opportunity for hydrology. In: Proceedings of ERAD, Helsinky

Jones DMA (1959) The shape of raindrops. J Meteorol 16(October):504–510

Marzano FS, Scaranari D, Celano M, Alberoni PP, Vulpiani G, Montopoli M (2006) Hydrometeor classification from dual-polarized weather radar: extending fuzzy logic from S-band to C-band data. Adv Geosci 7:109–114

Marzano FS, Scaranari D, Vulpiani G, Montopoli M (2008) Supervised classification and estimation of hydrometeors using C-band dual-polarized radars: a Bayesian approach. IEEE Trans Geosci Remote Sens 46:85–98

Mishchenko MI (2000) Calculation of the amplitude matrix for a nonspherical particle in a fixed orientation. Appl Opt 39:1026–1031

Mishchenko MI, Hovenier JW, Travis LD (eds) (2000) Light scattering by nonspherical particles: theory, measurements, and applications. Academic Press, San Diego, CA

Mishchenko MI, Travis LD (1998) Capabilities and limitations of a current Fortran implementation of the T-Matrix method for randomly oriented, rotationally symmetric scatterers. J Quant Spectros Radiative Transfer 60(3):309–324

Probert-Jones JR (1962) The radar equation in meteorology. Q J R Meteorol Soc 88:485–495

Pruppacher HR, Beard KV (1970) A wind tunnel investigation of the internal circulation and shape of water drops falling at terminal velocità in air. Q J R Meteorol Soc 96(April):247–256

Pruppacher HR, Pitter RL (1971) A semi-empirical determination of the shape of cloud and rain drops. J Atmos Sci 28(January):86–94

Ryzhkov AV, Schuur TJ, Burgess DW, Heinselman PL, Giangrande SE, Zrnić DS (2005) The joint polarization experiment. Polarimetric rainfall measurements and hydrometeor classification. Bull Am Meteorol Soc 86(6):809–824

Sachidananda M, Zrnic DS (1987) Rain rate estimates from differential polarization measurements. J Atmos Ocean Technol 4:588–598

Saffle R, Istok M, Johnson LD (2002) NEXRAD product improvement – progress and plans. In: Preprints of 18th international conference on IIPS, Orlando, FL, Am Meteorol Soc. Paper 5.1

Sauvageot H (1992) Radar meteorology. Artec House, Boston, MA

Straka JM, Zrnić DS, Ryzhkov AV (2000) Bulk hydrometeor classification and quantification using polarimetric radar data: synthesis of relations. J Appl Meteorol 39(8):1341–1372

Testud J, Le Bouar E, Obligis E, Ali-Mehenni M (2000) The rain profiling algorithm applied to polarimetric weather radar. J Atmos Ocean Technol 17(3):332–356

Toshiaki K, Iguchi T, Shimomai T, Kashiwagi N (2009) Raindrop size distribution modeling from a statistical rain parameter relation and its application to the TRMM precipitation radar rain retrieval algorithm. J Appl Meteorol Climatol 48(4):716–724

Ulaby FT, Moore RK, Fung AK (1986) Microwave remote sensing, active and passive. From theory to applications. vol III. Artech House, Boston, MA

Vivekanandan J, Zhang G, Brandes E (2004) Polarimetric radar estimators based on a constrained gamma drop size distribution model. J Appl Meteorol 43(2):217–230

Vivekanandan J, Zrnić DS, Ellis SM, Oye R, Ryzhkov AV, Straka J (1999) Cloud microphysics retrieval using S-band dual-polarization radar measurements. Bull Am Meteorol Soc 80(3):381–388

Vulpiani G, Marzano FS, Chandrasekar V, Lim S (2005) Constrained iterative technique with embedded neural-network for dual-polarization radar correction of rain path attenuation. IEEE Trans Geosci Remote Sens 43(10):2305–2314

Waterman PC (1971) Symmetry, unitarity, and geometry in electromagnetic scattering. Phys Rev D 3:825–839

Zrnic DS, Ryzhkov A (1998) Observations of insects and birds with polarimetric radar. IEEE Trans Geosci Remote Sens 36:661–668

Zrnić DS, Ryzhkov AV, Straka J, Liu Y, Vivekanandan J (2001) Testing a procedure for automatic classification of hydrometeor types. J Atmos Ocean Technol 18(6):892–913

http://www.springer.com/978-3-642-12967-4

Integrated Ground-Based Observing Systems
Applications for Climate, Meteorology, and Civil Protection

Cimini, D.; Marzano, F.S.; Visconti, G. (Eds.)
2011, XIII, 309 p., Hardcover
ISBN: 978-3-642-12967-4